ELSEVIER

Contents lists available at ScienceDirect

Colloids and Surfaces B: Biointerfaces

journal homepage: www.elsevier.com/locate/colsurfb





A Novel Anderson-Evans Polyoxometalate-based Metal-organic Framework Composite for the Highly Selective Isolation and Purification of Cytochrome C from Porcine Heart

Yang Zhang ^{a,1}, Dandan Zhang ^{b,1}, Xi Wu ^d, Ruizhi Song ^a, Xiaonan Zhang ^c, Mengmeng Wang ^a, Shaoheng He ^c, Qing Chen ^{a,c,*}

- ^a School of Pharmacy, Shenyang Medical College, Shenyang 110034, People's Republic of China
- ^b School of Public Health, Shenyang Medical College, Shenyang 110034, People's Republic of China
- ^c Translational Medicine Research Centre, Shenyang Medical College, Shenyang 110034, People's Republic of China
- ^d College of Chemistry, Liaoning University, Shenyang 110036, People's Republic of China

ARTICLE INFO

Keywords: Anderson-Evans polyoxometalate Metal-organic framework Cytochrome C Separation and purification Solid phase extraction

ABSTRACT

Anderson-Evans type polyoxometalate group (Na₆[TeW₆O₂₄]·22 H₂O, TeW₆) was combined with porous metalorganic framework ZIF-8 by electrostatic interaction to obtain a novel Anderson-Evans polyoxometalate-based metal-organic framework composite, TeW₆ @ZIF-8. FT-IR, Raman, XRD, TG, DSC, SEM, and TEM were used to characterize the composite. It was proved that the Anderson-Evans type polyoxometalate group TeW6 was successfully hybridized with metal-organic framework ZIF-8, and the composite possesses good stability. Based on the potential interaction between TeW6 and proteins and the coordination between imidazole groups in ZIF-8 and proteins with a porphyrin ring structure, the adsorption selectivity towards different proteins on the TeW6 @ZIF-8 composite was studied in this work. The experiment results showed that the TeW₆ @ZIF-8 composite was selectively adsorbed to cytochrome C. At pH 11.0, the adsorption efficiency of 94.01% was obtained for processing 1.0 mL 100 µg mL¹ cytochrome C with 3.0 mg TeW₆ @ZIF-8 composite. The adsorption behavior of cytochrome C fits well with the Langmuir adsorption model, corresponding to a theoretical adsorption capacity of 232.56 mg g⁻¹. The retained cytochrome C could be readily recovered by 1% SDS (m/m), giving rise to a recovery of 65.6%. Circular dichroism spectra indicate no conformational change for cytochrome C after the adsorption and desorption processes, demonstrating the favorable biocompatibility of TeW6 @ZIF-8 composite. In applying practical samples, SDS-PAGE results showed that cytochrome C was successfully isolated and purified by TeW6 @ZIF-8 composite from porcine heart protein extract, which is further identified with LC-MS/MS. Thus, a new strategy for separating and purifying cytochrome C from the porcine heart using TeW₆ @ZIF-8 composite as an adsorbent was established.

1. Introduction

Polyoxometalates (POMs) are a large family of anionic metal-oxygen clusters of the early transition metals in high oxidation states that exhibit unique and applicable physical and chemical properties [1,2]. They have interesting features in terms of molecular composition, size, solubility, shape, charge density, redox potential. In addition, they also have extensive applications in catalysis, electricity, magnetism, photochromism, biology, medicine, and materials science [3–6]. While POMs

initially mainly attracted the attention of chemists, they have recently piqued the curiosity of biochemists [7]. The high negative charge, large size, shape, and water-solubility of POMs allow them to bind to proteins [8]. Therefore, the research interests about POM have been focused on the molecular interactions between POMs and protein species [9,10]. Here, an Anderson-Evans type POM, specifically $Na_6[TeW_6O_{24}]\cdot 22~H_2O$ (TeW₆), has been frequently used as a protein crystallization additive [11–13]. Its effects on protein crystallization have been demonstrated with lysozyme, where negatively charged TeW_6 binds to sites with

^{*} Correspondence to: School of Pharmacy and Translational Medicine Research Centre, Shenyang Medical College, No.146 Huanghe North Avenue, Shenyang 110034, P. R. China.

E-mail address: chenqing.0906@163.com (Q. Chen).

 $^{^{\}rm 1}$ Yang Zhang and Dandan Zhang contributed equally to this work.

positive electrostatic potential located between two (or more) symmetry-related protein chains [14]. In addition, the mushroom tyrosinase *ab*PPO₄ crystallized in the space group as a crystallographic heterodimer composed of a polypeptide chain of L-TYR (Ser2-Thr556), a chain of A-TYR (Ser2-Ser383), and two half TeW₆ [15].

Metal-organic framework (MOF) is an excellent porous functional material with regularity and topological structure, which makes itself quite superior in terms of high specific surface area, adjustable structure, good thermal stability, low cost, and easy recovery [16,17]. Zeolitic imidazolate framework (ZIF) is a subfamily of the MOF that presents a zeolite-like crystalline topology [18]. Among them, ZIF-8 [Zn(mim)₂], formed by zinc ion as metal ion and 2-methylimidazole (mim) as ligand, has been widely studied due to its better thermal, hydrothermal and chemical stabilities [19,20]. Hence, ZIF-8 has attracted increasing attention in many applications such as catalysts, adsorption, separation and other fields [21-23]. To the best of our knowledge, combining ZIF-8 crystals with other materials can yield functional composites that exhibit new properties and broad application prospects in sensing electrocatalysts, drug delivery, and other biotechnologies [24-29]. For instance, biomineralized metal-organic framework nanoparticles (ZIF-8 NPs) were developed as biosensors for sensitive detection of flap endonuclease 1 (FEN1), which could be an effective strategy for cancer diagnosis [25]. Biodegradable ultrathin nanocapsules (NCs) based on catechol-modified gelatin and the ZIF-8 templates were engineered for selective delivery of drugs into bone [29].

Metal-organic frameworks based on different types of polyoxometalate present intriguing structures, excellent properties, and corresponding applications and their special applications in the fields of gas storage, separation, catalysis and drug delivery have attracted great research interests [30-33]. In addition, POMs can provide a variety of shapes, sizes, charges, and symmetries assemble various MOFs, and POM's adjustable acid/base, redox, and catalysis properties can also optimize MOFs for target application [34]. For example, a novel zeolitic polyoxometalate-based metal-organic [NBu₄]₃[PMoV₈MoV_{I4}O₃₆(OH)₄ Zn₄(BDC)₂]·2 H₂O (Z-POMOF1) exhibited remarkable electroactivity in the reduction of bromate, owing to the POM cations play the role of counterions and space-filling agents in the 3D MOF [35]. Song et al. proved that Keggin-type POM [CuPW₁₁O₃₉]⁵⁻ can be tightly embedded in the pores of MOF-199, which greatly enhances the catalytic performance of mercaptan oxidation to disulfide and hydrogen sulfide removal [36]. Furthermore, the extensive activity of POMs may be further exploited if they can be retained in the insoluble metal-organic frameworks, opening avenues in protein separation and purification of proteins.

Cardiac myocyte apoptosis, known as programmed cell death, plays an important role in the pathophysiology of many cardiac disorders such as heart failure, essential hypertension, and arrhythmia [37]. Mitochondria are potentially important in cardiac myocyte apoptosis, and mitochondrial structure and function changes occur when cardiomyocytes are apoptotic [38,39]. Cytochrome is a soluble protein in the membrane space of mitochondria, which is loosely attached to the surface of the inner membrane of mitochondria. When it migrates to the mitochondria, it combines with hemoglobin to form complete cytochrome C. One of the ways cell apoptosis is activated is by releasing cytochrome C from the mitochondria into the cytosol [40]. A study has shown that cells can protect themselves from apoptosis by blocking the release of cytochrome C using Bcl-xL [41]. Another way that cells can control apoptosis is by phosphorylation of Tyr48, which would turn cytochrome C into an anti-apoptotic switch [42]. To further reveal the secrets of apoptosis and clarify the mechanism of cytochrome C in apoptosis, cytochrome C must be isolated from biological samples to determine its differences. Consequently, it is of great significance for us to further explore the occurrence and prevention of heart disease.

In this paper, an Anderson-Evans type POM/MOF composite was designed and synthesized with Anderson-Evans type TeW $_6$ and ZIF-8 as raw materials, and the adsorption behavior of cytochrome C was studied

in depth. This study established a new route for the separation and purification of cytochrome C from the porcine heart using TeW $_6$ @ZIF-8 composite as adsorbent. It also opened up new applications of Anderson-Evans type POM/MOF composites in separation science and biotechnology.

2. Experimental

2.1. Materials

Unless otherwise stated, all chemicals used in this study were at least of analytical reagent grade. Cytochrome C (Cyt-C), bovine serum albumin (BSA), hemoglobin (Hb), and myoglobin (Mb) were purchased from Sigma-Aldrich (St. Louis, MO, USA). Zn(NO₃)₂.6 $\rm H_2O$, $\rm H_6TeO_6$, Na₂WO₄.2 $\rm H_2O$, NaCl, H₃PO₄, H₃BO₃, HCl, acetic acid, 2-methylimidazole, ethanol, methanol, imidazole, tris(hydroxymethyl)aminomethane (Tris), sodium dodecyl sulfate (SDS), and Coomassie brilliant blue G-250 were obtained from Sinopharm Chemical Reagent Co. Ltd. (Shanghai, China). The protein molecular weight marker (low, 3595 A, Takara Biotechnology Co., Ltd., Dalian, China) was a mixture of six purified proteins (phosphorylase b, MW 97.2 kDa; serum albumin, MW 66.4 kDa; ovalbumin, MW 44.3 kDa; carbonic anhydrase, MW 29.0 kDa; trypsin inhibitor, MW 20.1 kDa; lysozyme, MW 14.3 kDa). Deionized water (ddH₂O) of 18 M Ω cm was used throughout all experiments.

2.2. Instrumentations

A FT-IR spectra were recorded using a Nicolet-6700 FT-IR spectrophotometer (Thermo Fisher Scientific, USA) with a KBr disk from 400 to 4000 cm⁻¹. Raman spectra were obtained on an XploRA ONE laser Raman spectrometer (Horiba Scientific, Ltd., France). XRD patterns were taken on a BRUCKER D8 ADVANCE x-ray diffractometer (Brucker, Germany). The thermal stability of the product is evaluated by using a NETZSCH STA 499 F5/F3 Jupiter simultaneous thermal analyzer (Netzsch, Germany). SEM images were taken on a HITACHI SU8020 scanning electron microscope (Hitachi, Japan), and energy dispersive spectrometer (EDS) analysis results were obtained by HORIBA EX350 (Horiba Scientific, Ltd., France). TEM images were taken on HITACHI H-7650 transmission electron microscope (Hitachi, Japan). The nitrogen adsorption-desorption isotherms are obtained by using an ASAP 2020HD88 (Micromeritics Instrument, USA). U-3900 UV-vis spectrophotometer (Hitachi, Japan) with a 1.0 cm quartz cell was used to detect protein quantitatively. LC/MS mass spectrometer used in this study were equipped with Easy nLC 1200 chromatographic system at a nanoliter flow rate (Thermo Fisher Scientific, USA) and Q-Exactive HF-X mass spectrometer (Thermo Fisher Scientific, USA).

2.3. Synthesis of the TeW₆ @ZIF-8 composite

2.3.1. Preparation of $Na_6[TeW_6O_{24}]\cdot 22~H_2O~(TeW_6)$

 TeW_6 was synthesized in the following way [43,44]. Firstly, 0.60 g of $H_6 TeO_6$ and 5.00 g of $Na_2 WO_4.2\ H_2 O$ were dissolved in 100 mL $H_2 O$. The pH was adjusted to 5.0 with 1 mol L^{-1} HCl. The resulting solution was heated at 100 °C. After a 25% reduction in volume, it was cooled, filtered, and crystallized at room temperature. Colorless crystals of TeW_6 were obtained after one week, filtered, and air-dried.

2.3.2. Preparation of ZIF-8

The metal-organic framework ZIF-8 was prepared by adopting the previously described method [45]. A mixture containing 3.3 g of 2-methylimidazole and 1.5 g of $\rm Zn(NO_3)_2.6~H_2O$ in 20 mL of methanol was stirred at room temperature for 24 h to gain a milky white suspension, which was then collected by centrifugation. The obtained solid was washed three times with methanol solution and dried overnight at 80 °C to acquire pure ZIF-8 solid.

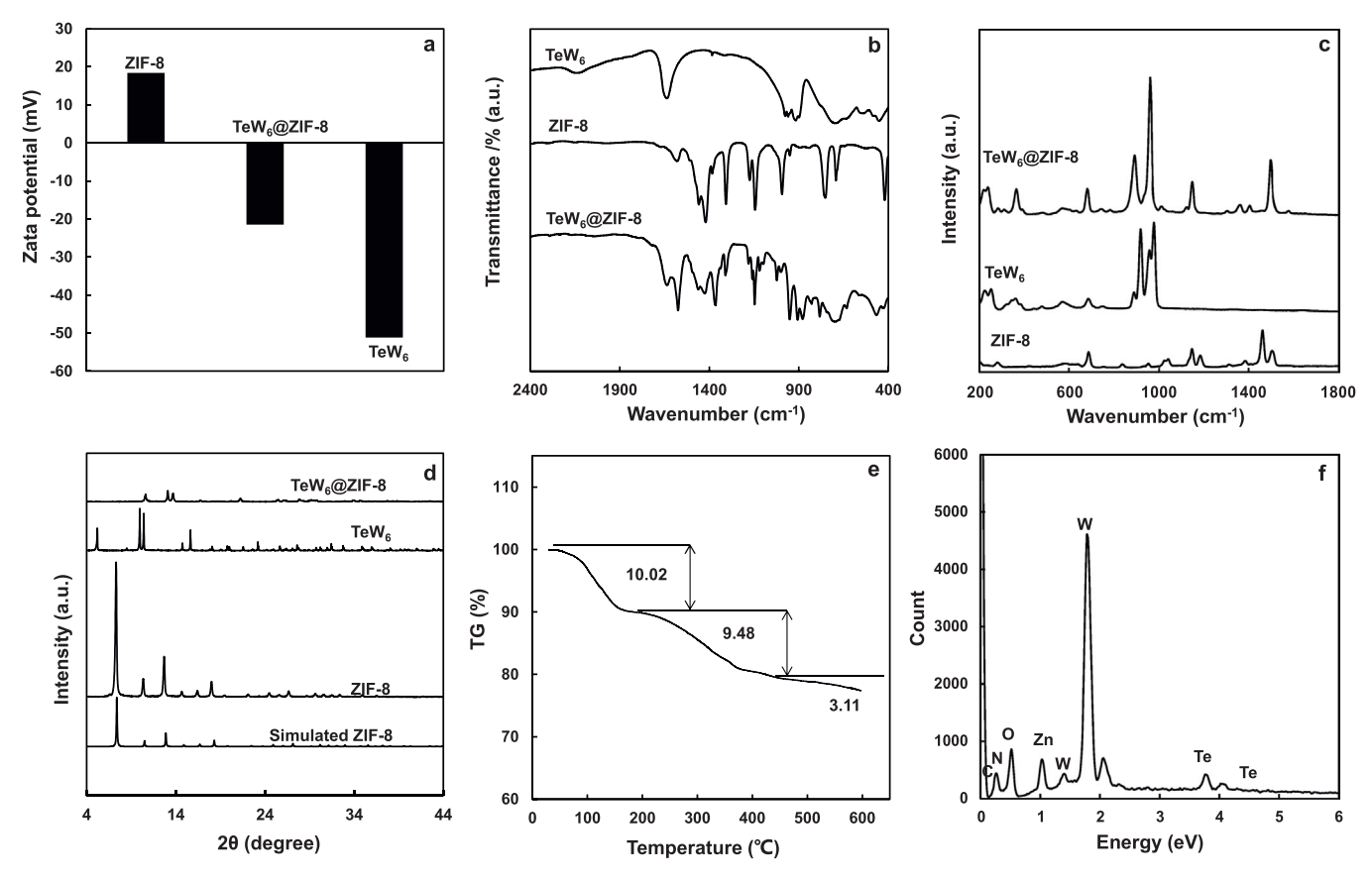


Fig. 1. The zeta potential of ZIF-8, TeW₆, and at neutral pH value (a). FT-IR spectra of ZIF-8, TeW₆ and TeW₆ @ZIF-8 (b). Raman spectra of ZIF-8, TeW₆, and TeW₆ @ZIF-8 (c). XRD patterns of ZIF-8, TeW₆, and TeW₆ @ZIF-8 and simulated ZIF-8 (d). TG analysis of TeW₆ @ZIF-8 in a N₂ atmosphere (e) and EDS analysis result for the TeW₆ @ZIF-8 composite (f).

2.3.3. Preparation of TeW₆ @ZIF-8 composite

Briefly, 0.1 g of ZIF-8 in 10 mL $\rm H_2O$ was added into a solution of 0.5 g of TeW₆ in 10 mL $\rm H_2O$, and the mixture was stirred at room temperature for 24 h. The color of the solution changed from a translucent white colloidal solution to a white suspension. The obtained solid is filtered, thoroughly washed with $\rm H_2O$, and dried at 80 °C for 12 h.

2.4. Adsorption/desorption of proteins by TeW₆ @ZIF-8 composite

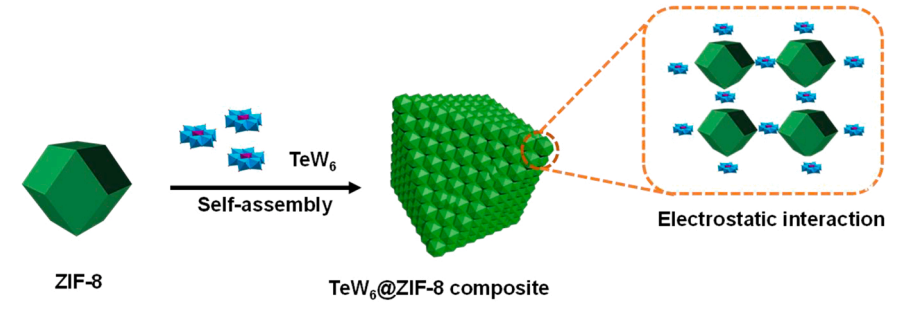
The adsorption behaviors of different types of protein models, namely, Cytochrome C (Cyt-C), bovine serum albumin (BSA), hemoglobin (Hb), myoglobin (Mb), on the TeW $_6$ @ZIF-8 composite were investigated. The acidity of the protein solutions was controlled by Britton-Robinson (BR) buffer in the range of 6.0–11.0.

In general, 1.0 mL of protein sample solution was mixed with 3.0 mg of TeW $_6$ @ZIF-8, and the mixture was shaken vigorously for 30 min to facilitate the adsorption of protein species. After centrifugation at 7000

rpm for 5 min, the supernatants of Cyt-C, Hb, and Mb were collected to quantify the residual protein content by monitoring the absorbance at 409 nm, and the supernatant of BSA was collected to quantify the residual protein content by monitoring the absorbance at 595 nm after binding with the Coomassie Brilliant Blue (Bradford method). The adsorption efficiency (E) was calculated by the following equation, where C_0 and C_1 represent the original and the residual protein concentrations, respectively.

$$E = \frac{C_0 - C_1}{C_0} \times 100\%$$

After the adsorption process, the TeW_6 @ZIF-8 composite was prewashed with 1.0 mL of ddH_2O to remove the non-specific adsorbed proteins. Afterward, 1.0 mL of 1%SDS (m/m) was added, and the mixture was oscillated for 15 min to strip the adsorbed proteins from the surface of the TeW_6 @ZIF-8 composite. After centrifugation at 7000 rpm for 5 min, the supernatant was collected for evaluating the elution



Scheme 1. Schematic illustration of the preparation of TeW₆ @ZIF-8 composite via electrostatic interaction between TeW₆ and ZIF-8.

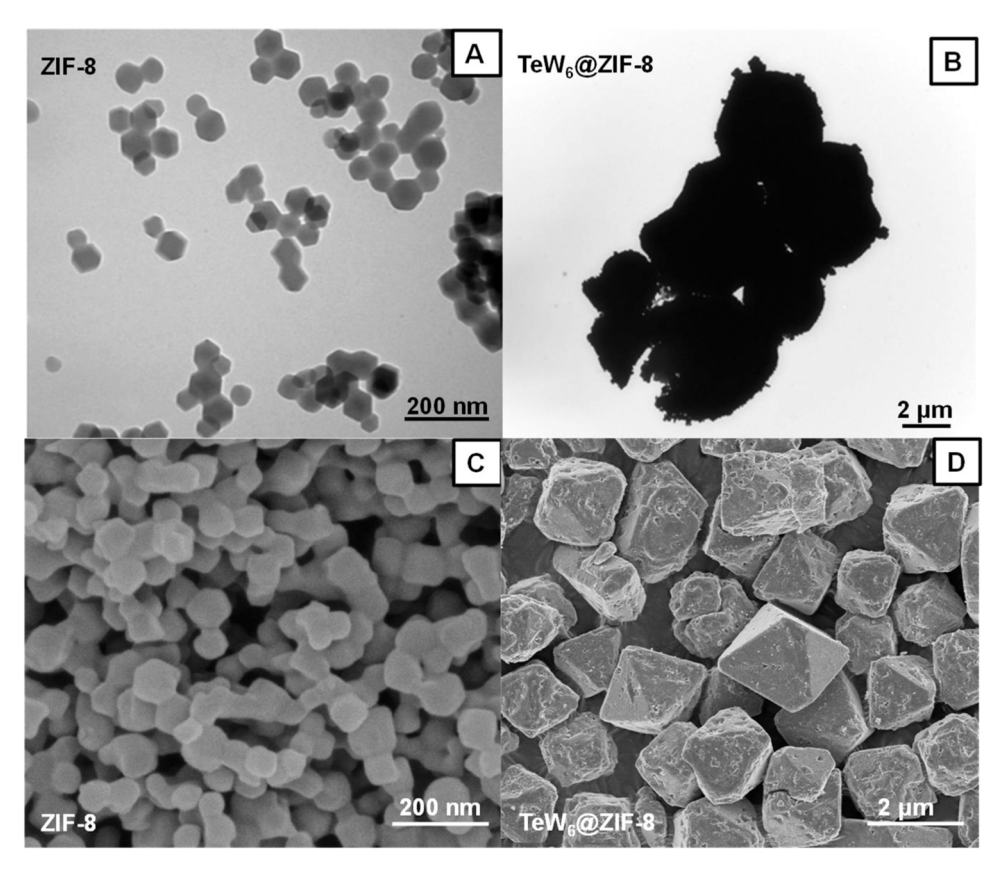


Fig. 2. TEM images of ZIF-8 and TeW₆ @ZIF-8 (A, B) and SEM images of ZIF-8 and TeW₆ @ZIF-8 (C, D).

efficiency or for subsequent studies.

2.5. Preparation of protein extraction from the porcine heart

The fresh porcine heart was obtained from the local market and washed with ddH_2O to remove blood. The heart was cut into small pieces with scissors, weighed 1.0 g, added to 200 mL of H_2O , and pounded with a mortar until minced. Then add 2.0 mol L^{-1} H_2SO_4 solution to adjust the pH value to 4.0, dilute to 500 mL, stir for 2 h. The resulting suspension was centrifuged at $10,000\, r/min$ for 5 min, and the precipitate was discarded. The supernatant was collected and concentrated for the ensuing study of protein adsorption by the TeW $_6$ @ZIF-8 composite.

3. Results and discussion

3.1. Characterization of the TeW₆ @ZIF-8 composite

The metal-organic framework composite based on Anderson-Evans POM was prepared by electrostatic interaction between the negatively charged TeW₆ and positively charged ZIF-8 (Fig. 1a). Due to the narrow size of the six-membered ring pores ($\sim\!3.4$ Å) [24] in ZIF-8, which was smaller than the size of the TeW₆ (10.269 $\times\!10.575 \times\!11.104$ Å) [44], TeW₆ could not easily be incorporated into the cavities of ZIF-8, resulting in the TeW₆ being bound to the surface of the ZIF-8 and further accumulating to form larger particle size of TeW₆ @ZIF-8 composite. (Scheme 1).

In order to prove the successful synthesis of TeW₆ @ZIF-8 composite and speculate its composition, structure and properties, FT-IR, Raman, XRD, TG, DSC and BET were made.

Fig. 1b shows the infrared spectra of the metal-organic framework ZIF-8, Anderson-Evans type tellurium tungstate TeW_{6} , and TeW_{6} combined metal-organic framework TeW_{6} @ZIF-8. In the infrared spectra of

ZIF-8, the peak at 1572 cm⁻¹, 1459 cm⁻¹, 1147 cm⁻¹, 421 cm⁻¹ were assigned to C=N stretching vibration, C-H stretching vibration, G-N stretching vibration, and the characteristic peak of Zn-N bond, respectively [22]. The absorption peaks at 957, 906, 772, 700, 549, and 461 cm⁻¹ demonstrated an Anderson-Evans structure for TeW₆ [43]. The infrared spectra of the new composite TeW₆ @ZIF-8 showed the characteristic peaks of TeW₆ and ZIF-8, which indicated that TeW₆ had been combined with ZIF-8 to form a new composite material. Meanwhile, the Raman spectrum of TeW₆ @ZIF-8 in Fig. 1c contains the typical \(\nu\)s (W=O) absorption bands of TeW₆ at 962 and 892 cm⁻¹ and the absorption bands at 1498, 1152, 679 cm⁻¹, which were consistent with the Raman peaks of ZIF-8.

In Fig. 1d, the sample XRD pattern of ZIF-8 had been clearly observed that the diffraction peaks of (001), (002), (112), (022), (013), (222), (114), (233), (134), (044), are identical with the simulated ZIF-8 [19] and it is shown that the product of ZIF-8 is purely phased, proving the formation of nanosized crystals. In addition, the XRD spectrum of TeW6 was also studied, which is similar to the crystal library data CCDC-632329 [44]. However, the main diffraction peak of TeW6 @ZIF-8 corresponds to the diffraction peak of TeW6 at 10.64° and the diffraction peak at 13.10° and 13.71° are the newly generated peak, which reveals the formation of new crystal complex.

Fig. 1e illustrates the results of the thermal decomposition analysis of TeW₆ @ZIF-8 composite. The thermogravimetry (TG) curve is roughly divided into three stages. In the first stage (RT-100 °C), the mass of the TeW₆ @ZIF-8 composite has dropped by 10.02%, which is due to the separation of small molecules such as water and methanol remaining on the composite surface or in the pore channels from the material after being heated. In the second stage (100–450 °C), 9.48% of the weight loss is attributed to the decomposition of organic matter (2-methyl-imidazole). In the third stage (500–600 °C), the metal oxide is gradually decomposed with the further increase of temperature [11]. Additionally, the EDS analysis result of the TeW₆ @ZIF-8 composite not only

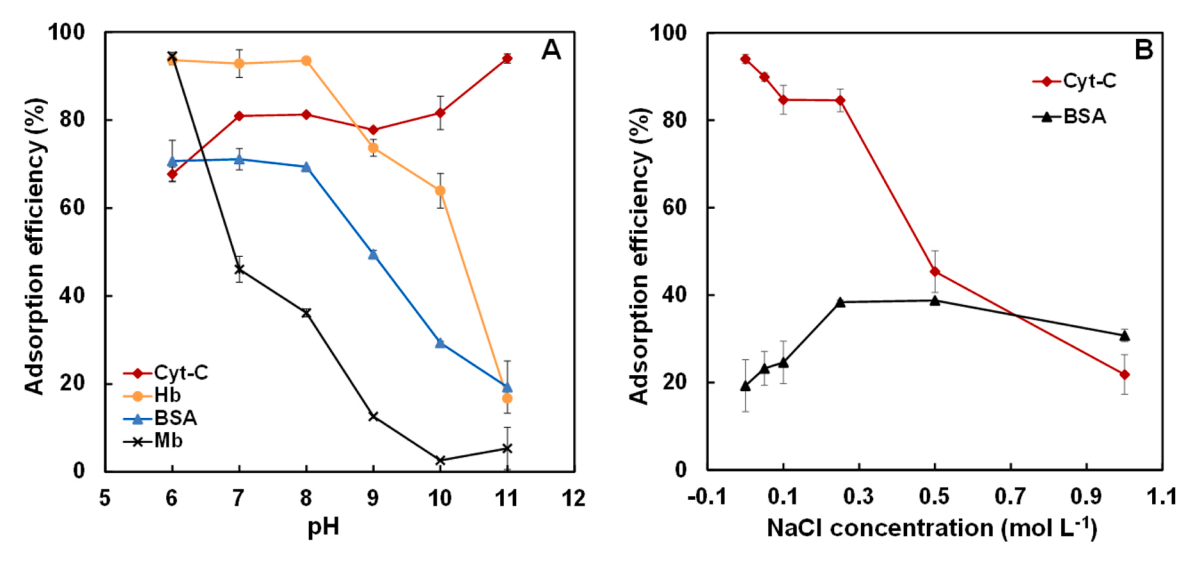


Fig. 3. pH-dependent adsorption behaviors of Cyt-C, Hb, BSA, and Mb onto TeW₆ @ZIF-8 surface (A); Effect of the ionic strength of the adsorption efficiency of Cyt-C, Hb, BSA, and Mb (B). Protein solution: 100 μg mL⁻¹, 1.0 mL; TeW₆ @ZIF-8: 3.0 mg.

identified C, N, and Zn for the part of ZIF-8, but also confirmed the presence of Te, W, and O of TeW $_6$ (Fig. 1f). The elemental analysis result of EDC of the product TeW $_6$ @ZIF-8 was shown in Table S1. These characterizations proved the successful synthesis of the TeW $_6$ @ZIF-8 composite simultaneously.

Fig. 2S shows the N_2 adsorption-desorption isotherms of ZIF-8 and TeW₆ @ZIF-8 measured at - 196 °C. The total adsorbed amount by ZIF-8 is similar to that previously reported [19]. Table S2 summarizes the textural properties of ZIF-8 and TeW₆ @ZIF-8, in particular the BET surface area, pore volume and pore size. Obviously, TeW₆ @ZIF-8 was found to have small specific surface area, reduced total pore volume and larger pore diameter. This is convincing evidence of the successful combination of TeW₆ and ZIF-8 layer by layer self-assembly.

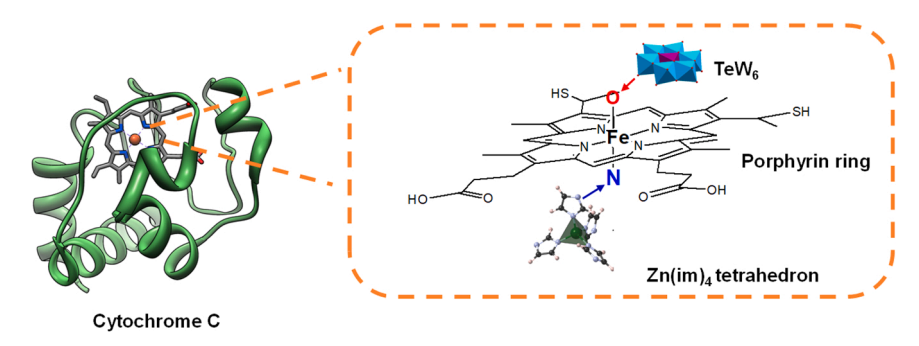
TEM and SEM are used to characterize the morphology, size and composition of the TeW $_6$ @ZIF-8 composite. Fig. 2A and B show the TEM images of ZIF-8 and TeW $_6$ @ZIF-8, respectively. Fig. 2A reveals that the particles of ZIF-8 were nanocrystals with sharp hexagonal facets, and the particle size was about 50–80 nm. After incorporating TeW $_6$ by electrostatic interactions and further molecules stacking, as shown in Fig. 2B, the size of the TeW $_6$ @ZIF-8 composite obtained was about 2–5 µm. The transmittance was significantly reduced, and the shape was no longer regular. Fig. 2C and D show the SEM images of ZIF-8 and TeW $_6$ @ZIF-8, respectively. In Fig. 2C, ZIF-8 is shown as uniform nanoparticles, which is consistent with the TEM images. After combining with TeW $_6$, a large number of micron particles were formed, most of which had uneven surface, and a few formed complete octahedral facets. (Fig. 2D).

3.2. Adsorption of proteins by TeW₆ @ZIF-8 composite

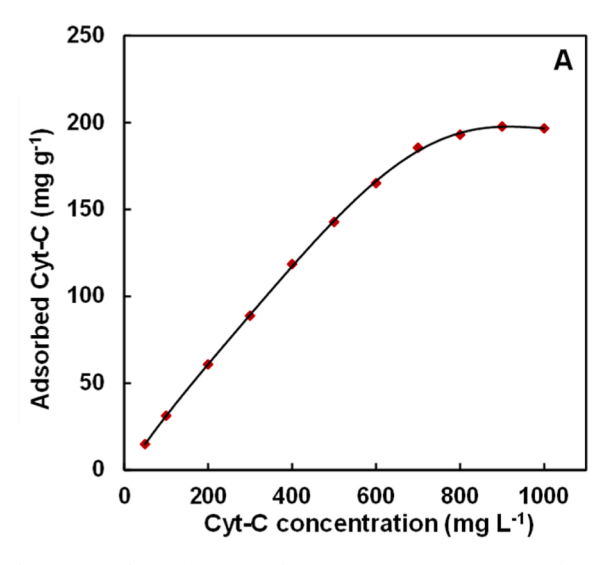
Protein is an amphoteric electrolyte with isoelectric point (pI). With the change of pH of solution, the charge properties of protein surface will change, and the interaction force with solid materials will also change. Therefore, the pH of the sample solution has a great influence on the adsorption behavior of protein on the surface of solid materials.

Cytochrome C (Cyt-C), hemoglobin (Hb), bovine serum albumin (BSA), and myoglobin (Mb) are the proteins in porcine heart cells with isoelectric points of 10.0, 7.1, 4.7, and 7.1, respectively. Among them, Cyt-C is a high-content protein in porcine heart cells. The TeW₆ @ZIF-8 composite exhibited poor stability under acidic conditions, while the composite was relatively stable under neutral and alkaline conditions. Therefore, the experiment mainly investigated the adsorption of these four proteins by the TeW6 @ZIF-8 composite within the pH range of 6.0-11.0. The adsorption efficiency of TeW₆ @ZIF-8 for Cyt-C, Hb, BSA, and Mb is shown in Fig. 3A. The adsorption efficiencies of Hb, BSA, and Mb decreased with the increase of pH value. When the pH reached 11, their adsorption efficiency dropped to less than 20%. The adsorption efficiency of Cyt-C was above 70% within the pH range of 6.0-11.0 and reached the maximum value of 94.01% when the pH value was 11.0. In conclusion, the selective separation of Cyt-C can be realized by selecting pH 11.0 as the adsorption condition.

Further, it was observed that the TeW_6 @ZIF-8 composite had high adsorption of Hb and Mb at pH 6.0, both exceeding 90%, which indicated that the TeW_6 @ZIF-8 composites had good adsorption capacity for Cyt-C, Hb and Mb. The common feature of these three proteins is that they all contain the heme structure with porphyrin, which consists of a ferrous complex of a sterically bulky derivative of tetraphenylporphyrin



Scheme 2. Interaction mechanism between cytochrome C and TeW₆ @ZIF-8 composite.



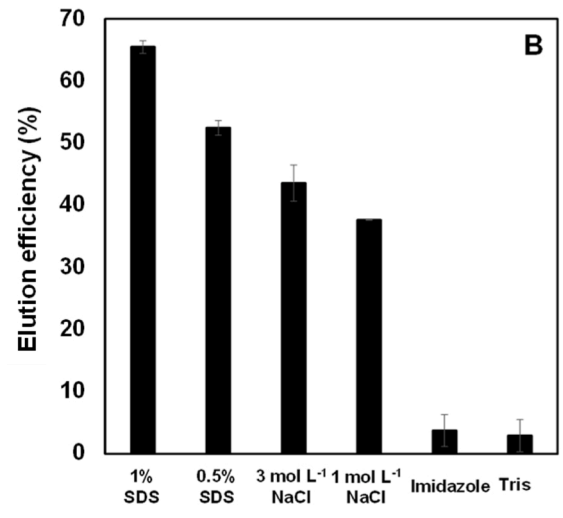


Fig. 4. The adsorption isotherm of Cyt-C on the TeW₆ @ZIF-8 composite(A); The recoveries of the adsorbed Cyt-C from TeW₆ @ZIF-8 composite using various buffers as stripping reagents (B). Cty-C solution: $100 \,\mu\text{g/mL}$, $1.0 \,\text{mL}$, pH 11.0; TeW₆ @ZIF-8: $3.0 \,\text{mg}$.

[46–50]. In the presence of an imidazole ligand, this ferrous complex reversibly binds O_2 . The O_2 substrate adopts a bent geometry and occupies the sixth position of the iron center [48]. The TeW_6 @ZIF-8 composite contains both imidazole ligand in ZIF-8 and oxygen in TeW_6 . Therefore, when the porphyrin rings of these three proteins are exposed to the environment, the composite shows a coordination binding with proteins. The iron atom in the porphyrin ring can be combined with oxygen in TeW_6 and the imidazole group in ZIF-8, as shown in (Scheme 2). However, due to electrostatic interaction, Hb and Mb are negative points under alkalinem conditions, and the repulsion with the TeW_6 @ZIF-8 composite leads to the decline of adsorption efficiency. Under the alkaline condition, pH 11.0 is close to the isoelectric point of Cyt-C, the protein is loosened, and the porphyrin ring is exposed, so high adsorption to Cyt-C is exhibited.

The ionic strength of the solution also has a great influence on the adsorption of protein. For proteins with different interaction mechanism with adsorbents, the effect of solution ionic strength on adsorption capacity is usually different. Under the condition of pH 11.0, a series of NaCl solutions with different concentrations were prepared to explore

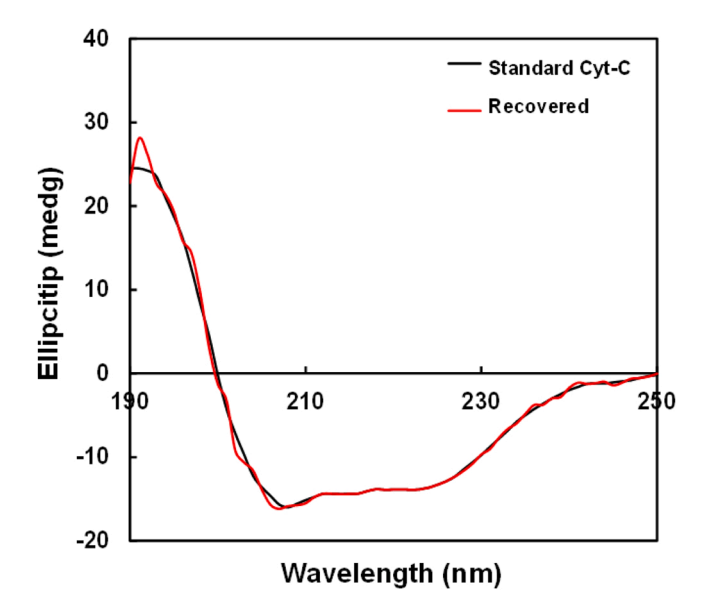


Fig. 5. CD spectra of Cyt-C standard solution and recovered Cyt-C after the capture/stripping process by use of TEW $_6$ @ZIF-8 in 1%SDS(B).

the influence of ionic strength on the adsorption efficiency of Cyt-C and BSA. The experimental results are shown in Fig. 3B. The ionic strength in the solution greatly influenced the adsorption of Cyt-C on the TeW₆ @ZIF-8 composite. With the increase of ionic strength, the adsorption efficiency of Cyt-C gradually decreased. Even so, it is worth mentioning that the adsorption efficiency of 80% can still be maintained in the range of 0-0.3 mol L-1 NaCl concentration. This indicates that the coordination is the main force for the adsorption of Cyt-C on the surface of TeW₆ @ZIF-8 composite under certain experimental conditions. With the increase of ionic strength, the competition between particles increased, which led to the decrease of Cyt-C adsorption efficiency. The adsorption efficiency of BSA gradually increased with the increasing salt concentration, indicating that the adsorption of BSA mainly depends on the hydrophobic force, which is due to the fact that the hydrophobicity of proteins can increase at certain salt concentrations. Because of the interference of certain salt concentrations in actual samples and increased adsorption selectivity of Cyt-C, a 0.04 mol L⁻¹ BR solution without NaCl was used in the subsequent experiment.

The effect of adsorption time on the adsorption efficiency of Cyt-C is shown in Fig. S1A. The adsorption efficiency of TeW $_6$ @ZIF-8 for Cyt-C rose gradually with the extension of the adsorption time, which increased rapidly in the first 25 min and then slowed down. Considering the adsorption and analytical efficiencies, the adsorption time was selected as 30 min. The effect of temperature of Cyt-C onto the TeW $_6$ @ZIF-8 was investigated in the range of 4–60 °C. As shown in Fig. S3, higher adsorption efficiency can be obtained between 15 °C and 25 °C (room temperature).

In order to investigate the adsorption capacity of TeW₆ @ZIF-8 for Cyt-C, the adsorption efficiency of Cyt-C at different concentrations (50–1000 μg mL) on the TeW₆ @ZIF-8 surface was investigated. As can be seen from Fig. 4A, the unit adsorption capacity of TeW₆ @ZIF-8 for Cyt-C gradually increased with the increase of Cyt-C concentration. When the Cyt-C concentration was greater than 700 μg mL $^{-1}$, the unit adsorption capacity of TeW₆ @ZIF-8 for Cyt-C remained stable, indicating that the adsorption capacity basically reached saturation. From the above, it can be seen that the adsorption of Cyt-C on TeW₆ @ZIF-8 surface was a single-layer adsorption, and the experimental data conformed to the *Langmuir* adsorption model. The equation is,

$$Q^* = \frac{Q_m \times C_e}{K_d + C_e}$$

which C_e (mg L⁻¹) as the protein concentration, Q^* (mg g⁻¹) as the amount of adsorbed protein at equilibrium, Q_m (mg g⁻¹) as the maximum

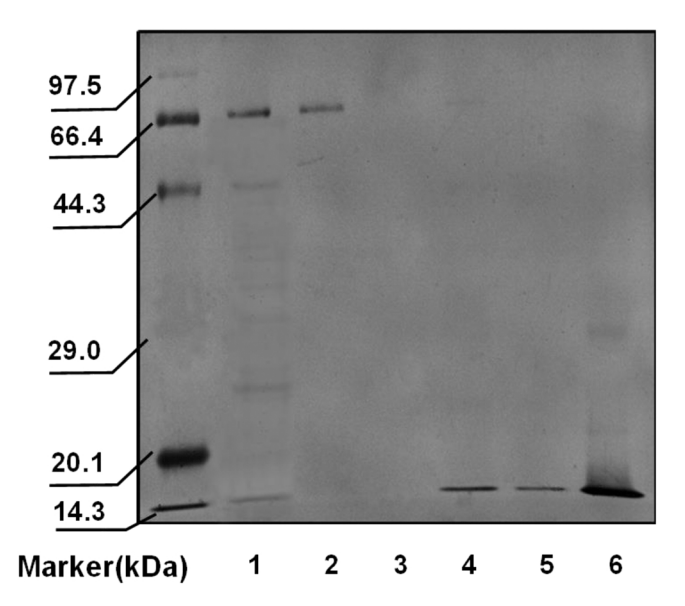


Fig. 6. Result of SDS-PAGE for the high isolation of Cyt-C from porcine heart protein extract.1: porcine heart protein extract; 2: 50-fold dilution of porcine heart protein extract after adsorption by the TeW₆ @ZIF-8 composite; 3: Prewashing solution collected by 0.04 mol $\rm L^{-1}$ BR buffer (at pH 11.0); 4: Cyt-C recovered by stripping with 200 μL 1% SDS solution; 5: Cyt-C recovered by stripping with 500 μL 1% SDS solution; 6: 100 μg mL $^{-1}$ of Cyt-C standard solution.

adsorption capacity and K_d as the adsorption constant. The maximum adsorption capacity Q_m of TeW₆ @ZIF-8 for Cyt-C can be obtained by plotting $1/q_{\rm eq}$ against $1/C_{\rm e}$. As shown in Fig. S1B, the linear equation is

 $1/q_{eq}{=}~0.1737~C_e~+0.0043,~$ and the correlation coefficient R^2 =0.09889. By fitting the experimental data to the Langmuir adsorption model, an adsorption capacity of 232.56 mg g $^{-1}$ is derived. In addition, the absorption capacity of TeW $_6$ @ZIF-8 to Cyt-C is significantly higher than that of the solid materials reported in the literature listed in Table S1

In order to effectively recover Cyt-C adsorbed on the surface of TeW_6 @ZIF-8, the type of eluent was selected in the experiment. The elution and recovery of Cyt-C adsorbed on TeW_6 @ZIF-8 by different elution agents, such as 1% SDS (m/m), 0.5% SDS, 3 mol L^{-1} NaCl, 1 mol L^{-1} NaCl, imidazole, and Tris solution were investigated, as shown in Fig. 4B. The results showed that the elution efficiency of Cyt-C by 50 mol L^{-1} Tris and 50 mol L^{-1} imidazole solution was lower than 10%. According to the influence analysis of ionic strength mentioned above, high salt concentration could reduce the adsorption efficiency of Cyt-C on the material surface, so 3 mol L^{-1} NaCl and 1 mol L^{-1} NaCl solutions had a certain elution efficiency. 1% SDS could achieve the maximum elution efficiency of 65.6%, and many studies showed that it would not change the secondary structure of the protein [51], so this study eventually chose 1% SDS as the elution agent for effective elution.(Fig. 5).

Protein conformational change is an important index to be considered in the process of protein separation, which is often studied by circular dichroism (CD) spectrum. In this experiment, an ultrafiltration centrifuge tube (Millipore, Amicon Ultra-4, 3 kDa) was used to remove SDS as much as possible and get pure Cyt-C through 10 times of centrifugation. As shown in Fig. 6, the CD curve of the final enriched Cyt-C is a typical β -fold, which is basically the same as that of the Cyt-C standard solution. The result showed that the whole adsorption and elution process had no irreversible damage to the secondary structure of Cyt-C. Therefore, the Cyt-C captured by TEW $_6$ @ZIF-8 is reliable for the subsequent applications and studies.

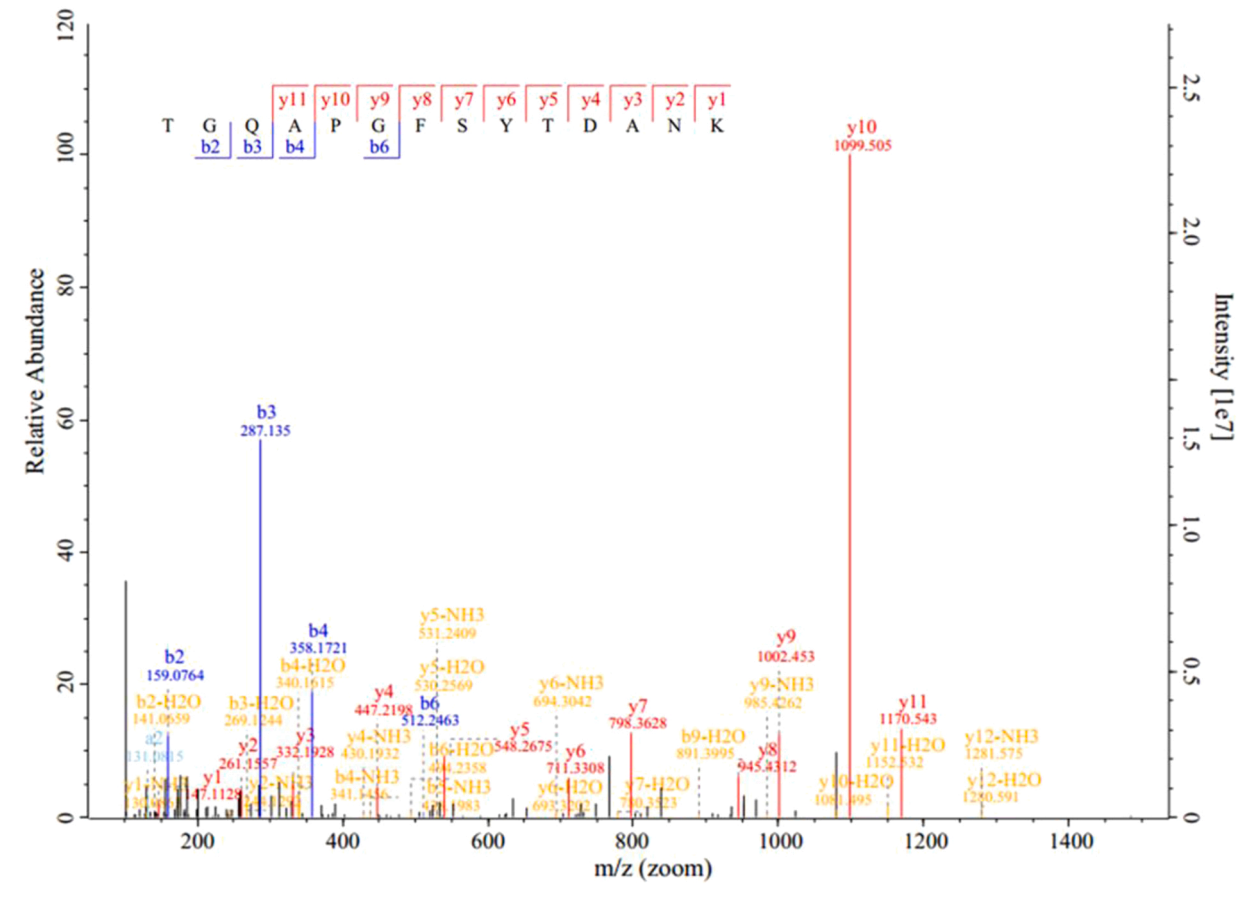


Fig. 7. Extracted ions of tryptic product peptides of Cyt-C by LC-MS/MS.

3.3. Separation and purification of cytochrome C from porcine heart by the TeW_6 @ZIF-8 composite

The practical applicability of the TeW₆ @ZIF-8 composite is the selective adsorption and isolation of Cyt-C from a complex biological sample matrix, namely, the porcine heart. The porcine heart protein extract was prepared using the method in the experimental part of the article. Then, the porcine heart protein extract was diluted 50-fold with $0.04 \; mol \; L^{-1} \; BR \; buffer \; (at \; pH \; 11.0) \; followed \; by \; centrifugation \; at$ 8000 rpm for 5 min. As described in the experimental section, the supernatant was then collected to undergo the adsorption/desorption processes with the TeW₆ @ZIF-8 composite. The SDS-PAGE analysis result is shown in Fig. 7. The porcine heart protein extract exhibited a few major bands within a range of molecular weight from 14.3 to 97.2 kDa (Lane 1), attributed mainly to serum albumin (66.4 kDa), Cyt-C (12.3 kDa), and other trace proteins. Lane 2 was the supernatant of 50fold dilution of porcine heart protein extract after adsorption by the TeW₆ @ZIF-8 composite. The protein band of Cyt-C in the supernatant became shallower at 12.3 kDa, which was almost invisible, while other bands did not change significantly. Lane 3 was collected as a prewashing solution by 0.04 mol L⁻¹ pH 11.0 BR buffer to wash away other proteins with non-specific and unstable adsorptions. As for the recovered solution, only one band at 12.3 kDa was observed using $200~\mu L$ and $500~\mu L$ 1% SDS and (m/m) solution as eluent (Lane 4 and Lane 5), which is consistent with that of the Cyt-C standard (Lane 6). This suggests the high purity of Cyt-C recovered from the porcine heart protein extract.

In order to identify the purified C, we used liquid chromatographymass spectrometry method (LC-MS/MS). Cyt-C has been sequenced and extensively studied, and its complete amino acid sequence can be found in the protein databases [52]. The theoretical tryptic peptides of Cyt-C were computationally predicted from the Uniprot Protein Data Bank using MaxQuant software. The characteristic peptides of Cyt-C were obtained by LC-MS/MS analysis of the trypsin digests. During LC-MS/MS analysis, the candidate peptide showed the corresponding molecular weight, which was consistent with the theoretical values. The corresponding sequence was TGQAPGFSYTDANK. (Fig. 6).

4. Conclusions

In this experiment, new metal-organic framework composites based on Anderson-Evans type polyoxometalate were successfully prepared by electrostatic interaction. The synthesized TeW₆ @ZIF composite was characterized by infrared spectroscopy, energy spectroscopy, Raman spectroscopy, X-ray diffraction, scanning electron microscopy, transmission electron microscopy, and thermogravimetry. Under the optimized experimental conditions, the TeW6 @ZIF composite showed a high selective adsorption capacity for cytochrome C. Thus, it provided practical feasibility for the selective isolation of cytochrome C from the porcine heart and obtained cytochrome C with high purity. The establishment of this method can accurately identify cytochrome C under different physiological conditions, which is of great significance for further exploring the mechanism and prevention of heart diseases. Therefore, the development of metal-organic frameworks based on different types of polyoxometalates, such as the Anderson-Evans type POM/MOF composite, can achieve the separation and purification of certain proteins with far-reaching applications.

Declaration of Competing Interest

The authors declare that they have no known competing financial interests or personal relationships that could have appeared to influence the work reported in this paper.

Acknowledgments

The authors appreciate financial supports from the Natural Science Foundation of China (21804093, 31900366, 82003693), PhD Start-up Foundation of Liaoning Province (2020-BS-266, 2021-BS-284), and the Science Research Foundation of Education Department for Liaoning Province (NO.SYYX202005).

Appendix A. Supporting information

Supplementary data associated with this article can be found in the online version at doi:10.1016/j.colsurfb.2022.112420.

References

- N.V. Izarova, M.T. Pope, U. Kortz, Noble Metals in Polyoxometalates, Angew. Chem. Int. Ed. 51 (2012) 9492–9510.
- [2] C. Jahier, S.S. Mal, R. Al-Oweini, U. Kortz, S. Nlate, DENDRI-POM Hybrids Based on the Keggin, Dawson, Preyssler and Venturello Polyanions and their Catalytic Evaluation in Oxidation Reactions, Polyhedron 57 (2013) 57–63.
- [3] R. Raza, A. Matin, S. Sarwar, M. Barsukova-Stuckart, M. Ibrahim, U. Kortzc, J. Iqbal, Polyoxometalates as Potent and Selective Inhibitors of Alkaline Phosphatases with Profound Anticancer and Amoebicidal Activities, Dalton Trans. 41 (2012) 14329–14336.
- [4] Z. Ilyas, H.S. Shah, R. Al-Oweini, U. Kortz, J. Iqbal, Antidiabetic Potential of Polyoxotungstates: in Vitro and in Vivo Studies, Metallomics 6 (2014) 1521–1526.
- [5] J. Iqbal, M. Barsukova-Stuckart, M. Ibrahim, S.U. Ali, U. Kortz, Polyoxometalates as Potent Inhibitors for Acetyl and Butyrylcholinesterases and as Potential Drugs for the Treatment of Alzheimer's Disease, Med. Chem. Res. 22 (2012) 1224–1228.
- [6] M.M. Wang, Q. Chen, D.D. Zhang, X.W. Chen, M.L. Chen, Tetra-nickel Substituted Polyoxotungsate as an Efficient Eorbent for the Isolation of His6-tagged Proteins from Cell Lysate, Talanta 171 (2017) 173–178.
- [7] M. Arefian, M. Mirzaei, H. Eshtiagh-Hosseini, A. Frontera, A Survey of the Different Roles of Polyoxometalates in their Interaction with Amino Acids, Peptides and Proteins, Dalton Trans. 46 (2017) 6812–6829.
- [8] B. Kowalewski, J. Poppe, U. Demmer, E. Warkentin, K. Schneider, Nature's Polyoxometalate Chemistry: X-ray Structure of the Mo Storage Protein Loaded with Discrete Polynuclear Mo-O Clusters, J. Am. Chem. Soc. 134 (2012) 9768–9774.
- [9] P. Schäfer, M. Krauss, N. Sträter, M. Zebisch, Structures of Legionella pneumophila NTPDase1 in Complex with Polyoxometallates, Acta Cryst. 70 (2014) 1147–1154.
- [10] N. Gumerova, L. Krivosudský, G. Fraqueza, J. Breibeck, E. Al-Sayed, E. Tanuhadi, A. Bijelic, J. Fuentes, M. Aureliano, A. Rompel, The P-type ATPase Inhibiting Potential of Polyoxotungstates, Metallomics 10 (2018) 287–295.
- [11] L. Vandebroek, H. Noguchi, K. Kamata, J. Tame, L.V. Meervelt, T.N. Parac-Vogt, A. Voet, Hybrid Assemblies of a Symmetric Designer Protein and Polyoxometalates with Matching Symmetry, Chem. Commun. 56 (2020) 11601–11604.
- [12] A. Bijelic, A. Rompel, Polyoxometalates: More than a Phasing Tool in Protein Crystallography, ChemTexts 4 (2018) 1–27.
- [13] I.R. Krauss, G. Ferraro, A. Pica, J. Marquez, J.R. Helliwell, A. Merlino, Principles and Methods Used to Grow and Optimize Crystals of Protein-Metallodrug Adducts, to Determine Metal Binding Sites and to Assign Metal Ligands, Metallomics 9 (2017) 1534–1547.
- [14] A. Bijelic, C. Molitor, S.G. Mauracher, R. Al-Oweini, U. Kortz, A. Rompel, Hen Egg-White Lysozyme Crystallisation: Protein Stacking and Structure Stability Enhanced by a Tellurium(VI)-Centred Polyoxotungstate, ChemBioChem 16 (2015) 233–241.
- [15] S.G. Mauracher, C. Molitor, R. Al-Oweini, U. Kortz, A. Rompel, Latent and Active abPPO4 Mushroom Tyrosinase Cocrystallized with Hexatungstotellurate(VI) in a Single Crystal, Acta Cryst. 70 (2014) 2301–2315.
- [16] R.J. Kuppler, D.J. Timmons, Q.R. Fang, J.R. Li, J.T.A. Makal, M.D. Young, D. Yuan, D. Zhao, W. Zhuang, H.-C. Zhou, Potential Applications of Metal-Organic Frameworks, Coord. Chem. Rev. 253 (2009) 3042–3066.
- [17] A. Salehabadi, N. Morad, M.I. Ahmad, A Study on Electrochemical Hydrogen Storage Performance of β-copper Phthalocyanine Rectangular Nanocuboids, Renew. Energy 146 (2020) 497–503.
- [18] J. Troyano, A. Carné-Sánchez, C. Avci, I. Imaz, D. Maspoch, Colloidal Metal–Organic Framework Particles: The Pioneering Case of ZIF-8, Chem. Soc. Rev. 48 (2019) 5534–5546.
- [19] Y. Pan, Y. Liu, G. Zeng, L. Zhao, Z. Lai, Rapid Synthesis of Zeolitic Imidazolate Framework-8 (ZIF-8) Nanocrystals in an Aqueous System, Chem. Commun. 47 (2011) 2071–2073.
- [20] O. Karagiaridi, M.B. Lalonde, W. Bury, A.A. Sarjeant, O.K. Farha, J.T. Hupp, Opening ZIF-8: a Catalytically Active Zeolitic Imidazolate Framework of Sodalite Topology with Unsubstituted Linkers, J. Am. Chem. Soc. 134 (2012) 18790–18796.
- [21] M. Zhang, Y. Yang, C. Li, L. Qian, C.T. Williams, C. Liang, PVP—Pd@ZIF-8 as Highly Efficient and Stable Catalysts for Selective Hydrogenation of 1,4-Butynediol, Catal. Sci. Technol. 4 (2014) 329–332.
- [22] F. Xie, Y. Wang, L. Zhuo, D. Ning, N. Yan, J. Li, S. Chen, Z. Lu, Multiple Hydrogen Bonding Self-Assembly Tailored Electrospun Polyimide Hybrid Filter for Efficient Air Pollution Control, J. Hazard. Mater. 412 (2021), 125260.
- [23] H. Fan, Q. Shi, H. Yan, S. Ji, J. Dong, G. Zhang, Simultaneous Spray Self-Assembly of Highly Loaded ZIF-8-PDMS Nanohybrid Membranes Exhibiting Exceptionally

- High Biobutanol-Permselective Pervaporation, Angew. Chem. 126 (2014)
- [24] R. Gao, Y. Lia, T. Zhu, Y. Dai, X. Li, L. Wang, L. Li, Q. Qu, ZIF-8@s-EPS as a Novel Hydrophilic Multifunctional Biomaterial for Efficient Scale Inhibition, Antibacterial and Antifouling in Water Treatment, Sci. Total Environ. 773 (2021), 145706.
- [25] Y. Tang, W. Wei, Y. Liu, S. Liu, Fluorescent Assay of FEN1 Activity with Nicking Enzyme-Assisted Signal Amplification Based on ZIF-8 for Imaging in Living Cells, Anal. Chem. 93 (2021) 4960–4966.
- [26] G. Lu, J.T. Hupp, Metal-Organic Frameworks as Sensors: A ZIF-8 Based Fabry-Perot Device as a Selective Sensor for Chemical Vapors and Gases, J. Am. Chem. Soc. 132 (2010) 7832–7833.
- [27] H. Zhong, J. Wang, Y. Zhang, W. Xu, W. Xing, D. Xu, Y. Zhang, X. Zhang, ZIF-8 Derived Graphene-Based Nitrogen-Doped Porous Carbon Sheets as Highly Efficient and Durable Oxygen Reduction Electrocatalysts, Angew. Chem. Int. Ed. 53 (2014) 1–7.
- [28] S. Mukhopadhyay, J. Debgupta, C. Singh, A. Kar, S.K. Das, A. Keggin, Polyoxometalate Shows Water Oxidation Activity at Neutral pH: POM@ZIF-8, an Efficient and Robust Electrocatalyst, Angew. Chem. Int. Ed. 57 (2018) 1918–1923.
- [29] X. Wang, D. Miao, X. Liang, J. Liang, C. Zhang, J. Yang, D. Kong, C. Wang, H. Sun, Nanocapsules Engineered from Polyhedral ZIF-8 Templates for Bone-Targeted Hydrophobic Drug Delivery, Biomater. Sci. 5 (2017) 658–662.
- [30] O.M. Yaghi, M. O'Keekffe, N.W. Ockwig, Reticular Synthesis and the Design of New Materials, Nature 423 (2003) 705–714.
- [31] C.N.R. Rao, S. Natarajan, R. Vaidhyanathan, Metal Carboxylates with Open Architectures, Angew. Chem. Int. Ed. 43 (2004) 1466–1496.
- [32] C.Y. Sun, S.X. Liu, D.D. Liang, K.Z. Shao, Y.H. Ren, Z.M. Su, Highly Stable Crystalline Catalysts Based on a Microporous Metal-Organic Framework and Polyoxometalates, J. Am. Chem. Soc. 131 (2009) 1883–1888.
- [33] F.J. Ma, S.X. Liu, D.D. Liang, G.J. Ren, Z.M. Su, Hydrogen Adsorption in Polyoxometalate Hybrid Compounds Based on Porous Metal-Organic Frameworks, Eur. J. Inorg. Chem. 24 (2010) 3756–3761.
- [34] F.J. Ma, S.X. Liu, C.Y. Sun, D.D. Liang, G.J. Ren, F. Wei, Y.G. Chen, Z.M. Su, A Sodalite-Type Porous Metal-Organic Framework with Polyoxometalate Templates: Adsorption and Decomposition of Dimethyl Methylphosphonate. J. Am. Chem. Soc. 133 (2011) 4178–4181.
- [35] L.M. Rodriguez-Albelo, A.R. Ruiz-Salvador, A. Sampieri, D.W. Lewis, B. Nohra, P. Mialane, A. Gomez, J. Marrot, F. Secheresse, C. Mellot-Draznieks, Zeolitic Polyoxometalate-Based Metal-Organic Frameworks (Z-POMOFs): Computational Evaluation of Hypothetical Polymorphs and the Successful Targeted Synthesis of the Redox-Active Z-POMOF1. J. Am. Chem. Soc. 131 (2009) 16078–16087.
- [36] J. Song, Z. Luo, D.K. Britt, H. Furukawa, O.M. Yaghi, K.I. Hardcastle, C.L. Hill, A. Multiunit, Catalyst with Synergistic Stability and Reactivity: A Polyoxometalate-Metal Organic Framework for Aerobic Decontamination, J. Am. Chem. Soc. 133 (2011) 16839–16846.

- [37] A. Abbate, G.G. Biondi-Zoccai, A. Baldi, Pathophysiologic Role of Myocardial Apoptosis in Post-Infarction Left Ventricular Remodeling, Cell. Physiol. 193 (2002) 145–153.
- [38] E. Chen, G. Proestou, D. Bourbeau, E. Wang, Rapid Up-regulation of Peptide Elongation Factor EF-1 Alpha Protein Levels is an Immediate Early Event During Oxidative Stress-induced Apoptosis, Exp. Cell Res. 259 (2000) 140–148.
- [39] S.A. Cook, P.H. Sugden, A. Clerk, Regulation of Bcl-2 Family Proteins During Development and in Response to Oxidative Stress in Cardiac Myocytes: Association With Changes in Mitochondrial Membrane Potential, Circ. Res. 85 (1999) 940–949.
- [40] D.J. Mcconkey, Y. Lin, L.K. Nutt, H.Z. Ozel, R.A. Newman, Cardiac Glycosides Stimulate Ca²⁺ Increases and Apoptosis in Androgen-independent, Metastatic Human Prostate Adenocarcinoma Cells, Cancer Res 60 (2000) 3807–3812.
- [41] J.M. García-Heredia, A. Díaz-Quintana, M. Salzano, M. Orzáez, E. Pérez-Payá, M. Teixeira, M. Rosa, I. Díaz-Moreno, Tyrosine Phosphorylation Turns Alkaline Transition into a Biologically Relevant Process and Makes Human Cytochrome c Behave as an Anti-Apoptotic Switch, Biol. Inorg. Chem. 16 (2011) 1155–1168.
- [42] S. Kharbanda, P. Pandey, L. Schofield, Role for Bcl-xL as an Inhibitor of Cytosolic Cytochrome c Accumulation in DNA Damage-Induced Apoptosis, PNAS 94 (1997) 6939–6942.
- [43] K.J. Schmidt, G.J. Schrobilgen, J.F. Sawyer, Hexasodium Hexatungstotellurate(VI) 22-Hydrate, Acta Crystallogr. C42 (1986) 1118–1120.
- [44] Z. Xu, P. Xi, F. Chen, Z. Zeng, Synthesis and Characterization of a Novel Anderson-Type Tungstotellurate Decorated by Transition Metal Complexes: [Na(H₂O)₃]₂[{Cu (2,2'-bipy)₂}₂(TeW₆O₂₄)]·4H₂O, Transit. Met. Chem. 33 (2008) 237–241.
- [45] H. Bux, F. Liang, Y. Li, J. Cravillon, M. Wiebcke, J. Caro, Zeolitic Imidazolate Framework Membrane with Molecular Sieving Properties by Microwave-Assisted Solvothermal Synthesis, J. Am. Chem. Soc. 131 (2009) 16000–16001.
- [46] Y.A. Vladimirov, E.V. Proskurnina, D.Y. Izmailov, A.A. Novikov, A.V. Brusnichkin, A.N. Osipov, V.E. Kagan, Mechanism of Activation of Cytochrome c Peroxidase Activity by Cardiolipin, Biochemistry 71 (2006) 989–997.
- [47] X. Kang, J. Carey, Role of Heme in Structural Organization of Cytochrome c Probed by Semisynthesis, Biochemistry 38 (1999) 15944–15951.
- [48] J.P. Collman, J.I. Brauman, T.R. Halbert, K.S. Suslick, Nature of O₂ and CO Binding to Metalloporphyrins and Heme Proteins, PNAS 73 (1976) 3333–3337.
- [49] H. Chen, M. Ikeda-Saito, S. Shaik, Nature of the Fe-O₂ Bonding in Oxy-myoglobin: Effect of the Protein, J. Am. Chem. Soc. 130 (2008) 14778–14790.
- [50] R.C. Hardison, A Brief History of Hemoglobins: Plant, Animal, Protist, and Bacteria, Proc. Natl. Acad. Sci. USA 93 (1996) 5675–5679.
- [51] D.D. Zhang, L.L. Hu, Q. Chen, X.W. Chen, J.H. Wang, Selective Adsorption of Hemoglobin with Polyoxometalate-derived Hybrid by Solidification of Superlacunary Phosphotungstate Polyoxoanions, Talanta 159 (2016) 23–28.
- [52] A.M. Hartley, N. Lukoyanova, Y. Zhang, A. Cabrera-Orefice, S. Arnold, B. Meunier, N. Pinotsis, A. Marechal, Structure of Yeast Cytochrome C Oxidase in a Supercomplex with Cytochrome bc1, Nat. Struct. Mol. Biol. 26 (2019) 78–83.